Vol. 7 • No. 5 • March 8 • 2017
www.advenergymat.de

ADVANCED ENERGY MATERIALS

WILEY-VCH

Single-Particle Performances and Properties of $LiFePO_4$ Nanocrystals for Li-Ion Batteries

Jiangtao Hu, Wen Li, Yandong Duan, Suihan Cui, Xiaohe Song, Yidong Liu, Jiaxin Zheng, Yuan Lin, and Feng Pan**

It has been recently reported that the solution diffusion, efficiency porosity, and electrode thickness can dominate the high rate performance in the 3D-printed and traditional $LiMn_{0.21}Fe_{0.79}PO_4$ electrodes for Li-ions batteries. Here, the intrinsic properties and performances of the single-particle (SP) of $LiFePO_4$ are investigated by developing the SP electrode and creating the SP-model, which will share deep insight on how to further improve the performance of the electrode and related materials. The SP electrode is generated by fully scattering and distributing $LiFePO_4$ nanoparticles to contact with the conductive network of carbon nanotube or conductive carbon to demonstrate the sharpest cyclic voltammetry peak and related SP-model is developed, by which it is found that the interfacial rate constant in aqueous electrolyte is one order of magnitude higher, accounting for the excellent rate performance in aqueous electrolyte for $LiFePO_4$. For the first time it has been proposed that the insight of pre-exponential factor of interface kinetic Arrhenius equation is related to desolvation/solvation process. Thus, this much higher interfacial rate constant in aqueous electrolyte shall be attributed to the much larger pre-exponential factor of interface kinetic Arrhenius equation, because the desolvation process is much easier for Li-ions jumping from aqueous electrolyte to the Janus solid–liquid interface of $LiFePO_4$.

1. Introduction

To improve the rate performance of $LiFePO_4$, an important commercial cathode material for rechargeable lithium ion batteries (LIBs), much effort has been devoted to understanding its electrochemical properties, such as the morphology modifying, carbon and ionic coating, metal doping, lithium intercalation and phase transformation, and influence of defects in the structure.[1] However, most of the properties are collected based on a realistic thick battery electrode, in which many nanoparticles with a broad distribution of particle sizes assemble. Recent experimental studies show that there is an ionic transport between adjacent crystallites that results from their redox potential difference during the delithiation,[2] which primarily originates from the dependence on thermodynamic properties on particle size.[3] The behavior of pressing the active material into thick slices or assembling to full battery can also lead to the coupling of stress with lithium chemical potential during the lithiation or delithiation process and introduce the concentration polarization, electrochemical polarization, and other internal interference within the electrode.[2,4] As a result, the obtained data based on thick battery electrode mainly reflect the properties of the collective particles with multipolarization effects.

Recently, we employed 3D printing to fabricate thin $LiMn_{0.21}Fe_{0.79}PO_4$ LIB electrodes, which show impressive electrochemical performance: a capacity of 108.45 mA h g^{-1} at 100 C and a reversible capacity of 150.21 mA h g^{-1} at 10 C after 1000 cycles.[5] We then demonstrated that except for the bulk Li-ion diffusion in cathode nanoparticles and particle interfacial reaction, the solution intrinsic diffusion coefficient, efficiency porosity, and electrode thickness could also dominate high rate performance of the cathode. However, the ultrathin electrodes are still composed of assembled $LiMn_{0.21}Fe_{0.79}PO_4$ nanocrystals and cannot reflect the intrinsic properties of a single nanoparticle, which would share deep insight to how to further improve the performance of electrode materials. Thus, to get the intrinsic properties of single nanocrystallites becomes our target in this work.

New testing method on this subject should be developed first. Recent progresses about this have been made to study the intercalation mechanism of $LiFePO_4$ nanocrystallites. Chueh et al. imaged ≈450 individual $LiFePO_4$ particles to confirm the particle-by-particle pathway during intercalation.[6] Brunetti et al. used precession electron diffraction to obtain $LiFePO_4$ and $FePO_4$ phase mapping at the scale of a particle and proved the domino-cascade model at the nanoscale level.[7] Li et al. track the migration of Li in $LiFePO_4$ electrodes with single particle sensitivity by using operando fluorescence-yield X-ray microscopy platform.[8] Using transmission electron microscopy and by the new electron forward scattering diffraction technique, Robert et al. unambiguously shows that the small particles delithiate first by the statistical analysis of 64000 $LiFePO_4$ particles.[9] Using

J. Hu, W. Li, Y. Duan, S. Cui, X. Song, Y. Liu, J. Zheng, Prof. Y. Lin, Prof. F. Pan
School of Advanced Materials
Peking University
Shenzhen Graduate School
Shenzhen 518055, People's Republic of China
E-mail: linyuan@iccas.ac.cn; panfeng@pkusz.edu.cn

DOI: 10.1002/aenm.201601894

an operando X-ray microscopy platform, Lim et al. mapped the dynamics of the Li composition and insertion rate within primary $LiFePO_4$ particles.[10] These methods share helpful insight into the Li intercalation/deintercalation kinetics within $LiFePO_4$ particles, but the method to test the intrinsic electrochemical properties of single $LiFePO_4$ nanocrystal is still lacking.

Cyclic voltammetry (CV) is a sensitive and is a widely used technique for the investigation of electrochemical kinetics. Given that Galvanostatic Intermittent Titration Technique (GITT) and Electrochemical Impedance Spectroscopy (EIS) are only applicable to solid-solution reaction system and cannot be applicable to $LiFePO_4$ due to its flat discharge platform,[11] and PITT measurement is relatively too complex, CV method would be a more appropriate method to study the kinetics of electrochemical performance of $LiFePO_4$. Most of studies using this method are simply taking advantage of the equation[11] $I_p = 2.69\times10^5 n^{\frac{1}{2}} A (D_{Li})^{\frac{1}{2}} v^{\frac{1}{2}} \Delta c_0$ (I_p: peak current; n: the electronic number participating in the reaction; A: the electrode area immersed in solution; D_{Li}: Li-ion diffusion coefficient; v: scan speed; C_0: concentration variations before and after the reaction) to evaluate diffusion coefficient[12] or electrochemical windows[13] and measure capacitance contribution.[14] We have employed CV fitting to obtain the relative parameters to demonstrate the reason why $LiFePO_4$ has ultrahigh rate performance in aqueous electrolytes.[15] Henstridge's group[16] derive a novel method for the direct extraction of kinetic data from experimental CV by numerical simulation, based on the Butler–Volmer (BV) function and the Fick's diffusion law. Furthermore, they introduce the asymmetric Marcus–Hush–Chidsey (MHC) theory to the study of surface-bound redox couples in CV curves and get the quantity of the reorganization energy and the asymmetry parameter on Tafel plots. However, almost all CV data in previous literatures are collected by tests on thick electrode or full battery to reflect the overall characteristic of the working electrode.[17] Though these findings are useful and scientifically meaningful to the practical utilization of the battery, to get accurate and quantitative information from the CV tests of a single nanocrystal would also be of fundamental interest and important for the practical utilization.

In this work, we developed a new method to form ultrathin single-particle (SP) electrode of $LiFePO_4$, in which $LiFePO_4$ nanoparticles could be fully scattered and distributed to contact with the conductive network of carbon nanotube (CNT) (or conductive carbon network). The sharpest CV peak of the SP electrode was obtained to study the intrinsic electrochemical properties of $LiFePO_4$ nanocrystals. We also developed a new SP-model for $LiFePO_4$ with the novelty that it can describe the relationship between reaction rate and voltage precisely by using data from the experimental potential-capacity (normalized as voltage vs state of charge (SOC)) curve of $LiFePO_4$ to replace the Nernst equation. By using this SP-model to fit the experimental CV curves of SP electrode of $LiFePO_4$, we finally get the diffusion coefficients and surface reaction coefficients of $LiFePO_4$ nanocrystals in the aqueous and organic electrolyte at different temperatures. The results quantitatively show that the intrinsic Li-ion diffusion coefficients of $LiFePO_4$ are nearly the same in water and organic electrolytes, but the interfacial rate constant in water electrolyte is one order higher than that in organic electrolyte, which can be the decisive factor for the excellent rate performance in aqueous electrolyte for $LiFePO_4$. By investigating the temperature effect of interfacial rate constant, the insight of pre-exponential factor and the active energy of the interfacial reaction equation can be understood for the first time, which are related with desolvation/solvation process and solid–liquid interface structure of $LiFePO_4$, respectively.

2. Results and Discussion

2.1. Preparation the SP Electrodes

Figure 1a shows the crystal structure of the synthesized $LiFePO_4$@C products, which exhibits a single-phase olivine-type structure with Pnma space group (JCPDS NO. 81-1173). Reitveld refinement of X-ray diffraction (XRD) data is conducted to identify the lattice constants and confirm that there are no impurity phases (Figure S1, Supporting Information). The scanning electron microscopy (SEM) pictures of $LiFePO_4$@C were shown in Figure 1b, and the mean particle size of $LiFePO_4$ is about 40 nm.

To prepare the SP $LiFePO_4$ electrode, some key factors, such as the time-scale of the ultrasonic dispersion of nanoparticles in slurry and the thickness of the electrode to achieve SP performance, were first investigated. We defined that the thin electrode with very sharp CV peaks whose electrode material has perfect particle dispersion with long ultrasonic time as SP electrode. During our experiments, we did CV tests in both aqueous and organic electrolytes using ultrathin electrodes with the slurry samples under different ultrasonic time (Figures S2 and S3, Supporting Information). Obviously, the CV peak changes sharper with the longer ultrasonic time, and the half-width nearly remains constant after 50 min ultrasonic. There would be lots of agglomeration with short ultrasonic time, as shown in Figures S4 and S5 of the Supporting Information. We also did Energy Dispersive Spectroscopy (EDS) measurement of slurry materials with 70 and 5 min ultrasonic time, as shown in Figure S6 of the Supporting Information, which did not show distinguished differences of element distributions due to the resolution limit. Then we take the 70 min ultrasonic slurry materials for further tests, which would be dispersed enough to form SP electrodes. The optimized amount of conductive carbon in the slurry creates conductive networks to reduce the resistance for electrodes and to separate $LiFePO_4$ nanocrystals as single-particle embedded in conductive carbon networks. In order to test the thickness of electrodes, we dropped the slurry (after ultrasonic for 70 min) on quartz monitor crystal with the ultrathin (nanoscale, about 100–200 nm thick, Figure S7, Supporting Information) and with normal thick (micrometer size, about 7 μm, Figure S8 of the Supporting Information and Figure 1c) electrodes, respectively. The CV performances of ultrathin electrodes formed with the deep-dispersed slurry (after ultrasonic for 70 min) kept sharpest, thus such type of electrode could be called as SP electrode in this study. Hence, to prepare the SP electrode, we should take care of two key factors: to form a thin electrode (eliminate the concentration polarization of electrode) and to take long ultrasound time for dispersing slurry to decrease agglomeration.

Figures S7a and S8a of the Supporting Information show the distribution of the prepared SP electrode and thick electrode dropped

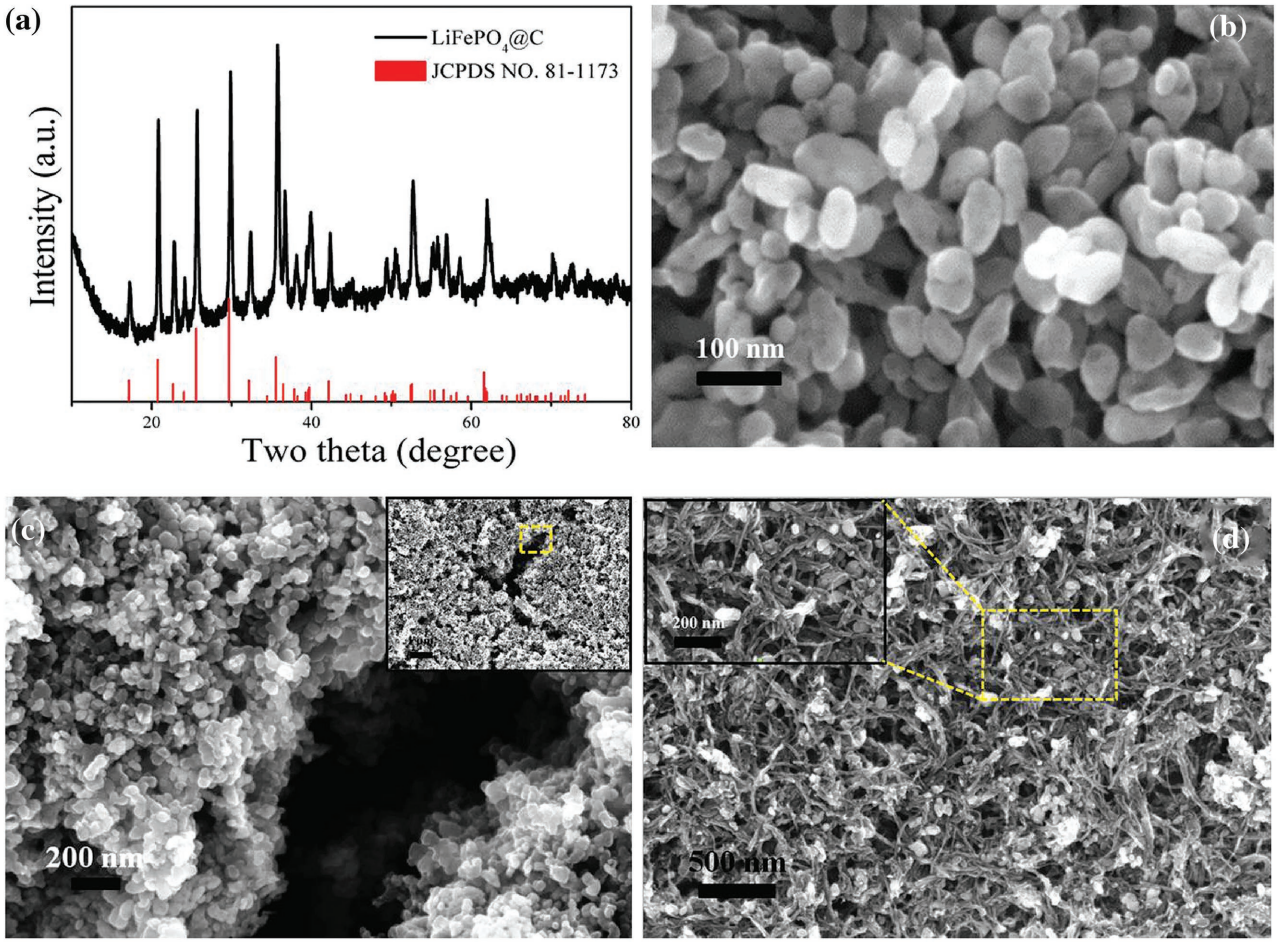

Figure 1. a,b) XRD and SEM data of $LiFePO_4$@C. c) The 3D confocal images of thick electrode dropped on quartz monitor crystals. d) The spatial structure of SP electrode using CNT.

on quartz monitor crystal by 3D confocal, and the height of the thin and thick electrode are nanoscale and micrometer size, respectively. Figure 1c and Figures S7 band S9 (Supporting Information) show the spatial structure and physical map of the two kinds of electrodes. Obviously, the SP electrode shows contacted nanoparticles ($LiFePO_4$ nanocrystals with mean size of about 40 nm) embedded in conductive carbon nanoparticles (also about 40 nm) to make a network with mesoporous (10–20 nm) and macroporous (100–500 nm), which can lead to each $LiFePO_4$ nanocrystal closely to contact with conductive network formed by conductive-carbon nanoparticles and electrolyte for electronic and Li-ion conduction sufficiently, respectively. Thus, the SP electrode could minimize the concentration polarization, electrochemical polarization, and other internal interference to benefit for testing the intrinsic electrochemical properties of $LiFePO_4$ single particles. Figure S10 of the Supporting Information displays the height distribution of electrode materials coating on quartz monitor crystals by step profiler. By contrast, the thick electrodes show a closely contacted nanoparticle-network with less mesoporous and macroporous, which would easily generate concentration polarization along the thick-direction of an electrode during the charging–discharging process of LIBs.

Similarly, we changed the carbon black to CNT with the ultrasonic time of 70 min. It can be seen that the $LiFePO_4$ nanoparticles could be scattered and distributed to contact with the CNT-network very well, as shown in Figure 1d. Additionally, we adjusted the proportion of $LiFePO_4$ nanocrystals and carbon black to realize an absolute single-particle electrode. Note that when we increased the ratio of carbon black to $LiFePO_4$ nanocrystals to more than 1:1 in weight, the CV curves expressed more capacitance information (Figure S11, Supporting Information). An optimized amount of conductive carbon black in our slurry not only reduces the resistance between the particles and the pole piece, but also can separate the $LiFePO_4$ particles and reduce the interparticle ionic or electronic transport limitation. Thus, conductive carbon nanoparticles can create the conductive networks, which play similar role as CNTs, to fully scatter and distribute $LiFePO_4$ nanoparticles to contact with the conductive networks, resulting in that both types of SP electrodes exhibit the sharpest CV curves.

2.2. Electrochemical Tests

CV tests were conducted on these two kinds of thick (or normal coin cells) and SP electrodes in different electrolytes circumstances. As the load of active materials was not exactly the same,

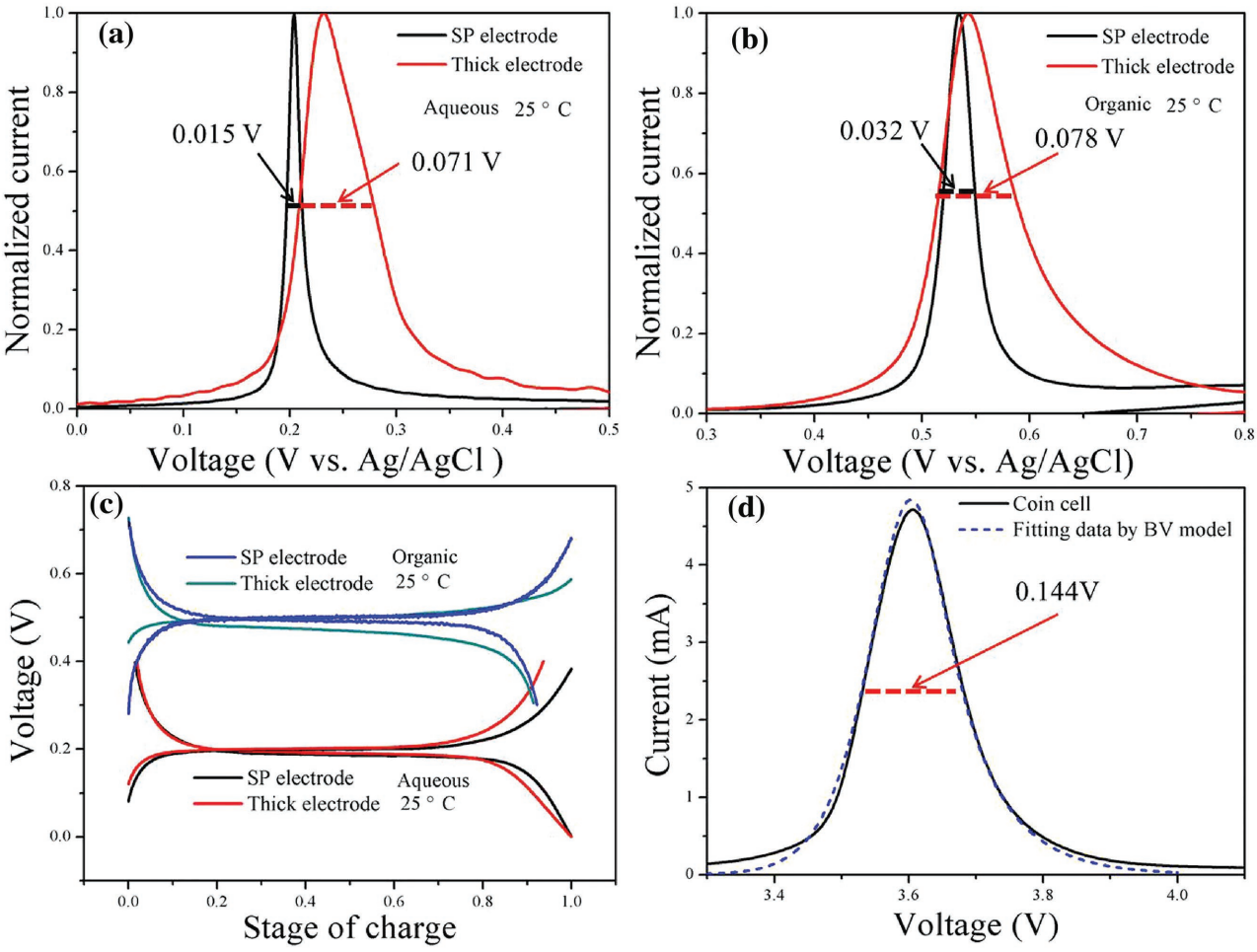

Figure 2. The CV data of SP electrode and thick electrode measured in a) aqueous and b) organic electrolyte at room temperature (25 °C) at 1 mV s^{-1}. c) The charge/discharge curves of SP electrode and thick electrode in aqueous and organic electrolyte at 0.2 C. d) The CV data of coin cell ($LiFePO_4$:C:PVDF = 7:2:1) at 1 mV s^{-1} and the fitting data by BV model.

the heights of CV peaks were a little different. In order to compare the changing trends of CV curves commodiously, we normalized them by divided the maximum value of each CV peaks, as shown in **Figure 2**a,b. Obviously, compared with the thick electrode and normal coin cell, it can be observed that the anodic peaks of SP electrode are very sharp, the half-width of SP electrode is much narrower, and the gradient of former's rising edge is also higher. Note that cathode peaks of SP electrode show the same kind of performances as shown in Figures S12 and S13 of the Supporting Information. Interestingly, we took charge/discharge potential-capacity tests for the two electrodes in aqueous and organic electrolytes at 0.2 C (1 C = 170 mA g^{-1}), respectively, and found that the discharge curves of SP electrode and thick electrode were almost coincident in both electrolytes (Figure 2c). So a question is aroused: why do the charge/discharge potential-capacity curves of SP and thick electrodes keep quite the same with the similar charge/discharge platform (about 80% capacities at almost same voltage), but the CV data show such a big difference between SP and thick electrodes, such as the full width at half maximum of CV for SP electrode and thick electrode 0.015 and 0.071 V in aqueous, and 0.032 and 0.078 V in organic electrolytes, respectively?

2.3. Improved SP Model

Generally, there are two kinds of CV simulation model: BV model and MHC model (see the Experimental Section). The CV curves of coin cells in organic electrolyte can be fitted well by numerical simulation based on BV model (Figure 2d), indicating the BV equation can be applied to thick electrodes of $LiFePO_4$. Then we adjusted the load transfer coefficient and diffusion coefficient of BV model and reaction constant of MHC, which determines the shape of CV, to fit the CV curves of SP electrodes in the two electrolytes. Surprisingly, even when we adjusted these factors to the limits, it is still impossible to fit the experimental curves well (Figure S14, Supporting Information). Obviously, the BV and MHC diffusion model is unsuitable to describe the SP electrode of $LiFePO_4$ nanocrystals.

For the simplified electrochemical reaction, we usually only considered the mass transfer process and interface charge transfer process. In previous CV analysis, the most commonly encountered mass transfer process was spreading in half infinite plane while the interface charge transfer process

is often described by the standard Butler–Volmer equation.[18,19] However, $LiFePO_4$ does not meet these two conditions, as $LiFePO_4$ is different from other cathode materials, such as Li(Ni, Co, Al, Mn)O_2, which exhibit the representative solid-solution "S" type in the characteristic of potential-capacity curves in large range at the room-temperature.[20] Moreover, in the cathode materials, the change of lithium concentration is evenly distributed in the process of charging and discharging,[21] while the lithium concentration change in the process of charging and discharging is uneven in $LiFePO_4$, and there is a significant platform in the potential-capacity curves. Note that the capacity can be indicated by SOC. As a result, the relationship between the potential and SOC that depicted by Nernst equation applied to Butler–Volmer system is not suitable for $LiFePO_4$. Besides, $LiFePO_4$ SP electrode is a finite spherical diffusion model that is inconsistent with the condition of half infinite plane spread. However, in the thick $LiFePO_4$ electrode, many nanoparticles with a broad distribution of particle sizes assemble to contact with each other. The ionic transport between adjacent crystallites and the coupling of stress with lithium chemical potential during the lithiation or delithiation process would lead to the concentration polarization, electrochemical polarization, and other internal interference within the electrode. Thus there exists concentration diffusion in the whole electrode, and the BV equation is appropriate to describe thick electrodes of $LiFePO_4$.

Based on the above analysis, we construct a new SP-model in this work which is composed of diffusion process and interface charge transfer process. During the oxidation process of CV scanning, the internal Li-ions within $LiFePO_4$ (LFP) particles begin to spread out, the diffusion process satisfies the Fick's diffusion law (Equation (1), the signification and units are depicted in Table 2)

$$\frac{\partial C(x,t)}{\partial t} = \frac{D_{\mathrm{Li}}}{x^2}\frac{\partial}{\partial x}\left(x^2\frac{\partial C(x,t)}{\partial x}\right) \tag{1}$$

As for the interface electron exchange process described in the Butler–Volmer equation (Equation (2)), the total reaction rate is equal to the oxidation rate constant (k_{Ox}) multiplied by the reduction state concentration ($C(R_s,t)$) and then minus the reduction rate constant (k_{Re}) multiplied by the oxidation state concentration ($C'(R_s,t)$)), which also suites to SP-model

$$i = \mathrm{FA}\left(k_{\mathrm{Ox}}C(R_s,t) - k_{\mathrm{Re}}C'(\mathrm{R_s,t})\right) \tag{2}$$

However, it should be noted that the reduction and oxidation reaction rate of $LiFePO_4$ SP electrodes cannot fitted by Nernst equation (Equations (3) and (4)). Also note that Nernst equation can be used in thick electrode of $LiFePO_4$ with concentration polarization, which could be attributed to the lithium concentration change in the process of charging and discharging due to interparticles' intercharge/discharge of $LiFePO_4$ in the thick eletrodes[5] and would perform similar to solid-solution cathode materials (Figure S15 (red line), Supporting Information)

$$k_{\mathrm{Re}} = k^0\exp\left\{-\alpha^{\circ}\frac{F}{\mathrm{RT}}\left[E-E^0\right]\right\} \tag{3}$$

$$k_{\mathrm{Ox}} = k^0\exp\left\{(1-\alpha)^{\circ}\frac{F}{\mathrm{RT}}\left[E-E^0\right]\right\} \tag{4}$$

The novelty of our SP model is the precise relationship between reaction rate and voltage (Equation (5)) which is got by using the real potential-capacity (normalized as voltage-SOC) curve of $LiFePO_4$ (Figure S15 black line, Supporting Information) to replace the Nernst equation, because the Nernst equation cannot describe potential-SOC curve for the $LiFePO_4$ nanocrystals SP electrodes

$$k_{Re} \propto -f\left(E(soc)\right),\ {}^{\infty}k_{Ox} \propto {}^{\circ}f\left(E(soc)\right) \tag{5}$$

$$K_{\mathrm{eq}} = \frac{k_{\mathrm{Ox}}}{k_{\mathrm{Re}}} = \frac{(1-\mathrm{SOC})}{\mathrm{SOC}} \tag{6}$$

By using the theory that reaction rate and the concentration (or SOC) of the activated complex are the positive relationship (Equation (6)) and adding Equations (5) and (6) into Equation (2), we can get the relationship between the voltage and current, then to simulate the CV data of SP electrode. (The detailed information about SP-model was described in the Experimental Section.) **Figure 3**a shows how D_{Li} affects the shape of a CV curve, such as the simulated CV curves with fixed parameters ($K^0 = 1\times10^{-8}$ cm s^{-1}, $\alpha = 0.5$) and tuning D_{Li} (from 1×10^{-15} to 5×10^{-14} cm^2 s^{-1}). We can see that when D_{Li} increases, the radian of falling edge of the CV curves is also increased and the trailing is vanished, but the half-width is almost kept in constant. Similarly, the trend of the change of CV shape with K^0 (from 1×10^{-9} to 5×10^{-8} cm s^{-1}) was shown in Figure 3b when other parameters were fixed ($D_{\mathrm{Li}} = 1\times10^{-14}$ cm^2 s^{-1}, $\alpha = 0.5$), in which the gradient of rising edge is increased obviously whereas half-width is diminished in the wake of increasing

Table 1. The simulation data of SP electrode at different temperatures in different electrolytes.

Parameters		Aqueous [°C]			Organic [°C]		
		0	25	50	0	25	50
D_{Li} (cm^2 s^{-1})	Charge	$>1.8\times10^{-14}$	$>2.8\times10^{-14}$	$>1.4\times10^{-14}$	$>1.5\times10^{-14}$	$>3.0\times10^{-14}$	$>3.0\times10^{-14}$
	Discharge	$>1.0\times10^{-14}$	$>2.0\times10^{-14}$	$>2.8\times10^{-14}$	$>1.5\times10^{-14}$	$>3.0\times10^{-14}$	$>3.1\times10^{-14}$
K^0 (cm s^{-1})	Charge	4.3×10^{-9}	2.0×10^{-8}	7.0×10^{-8}	8.0×10^{-10}	3.0×10^{-9}	9.0×10^{-9}
	Discharge	4.0×10^{-9}	1.8×10^{-8}	6.0×10^{-8}	7.0×10^{-10}	3.0×10^{-9}	9.0×10^{-9}

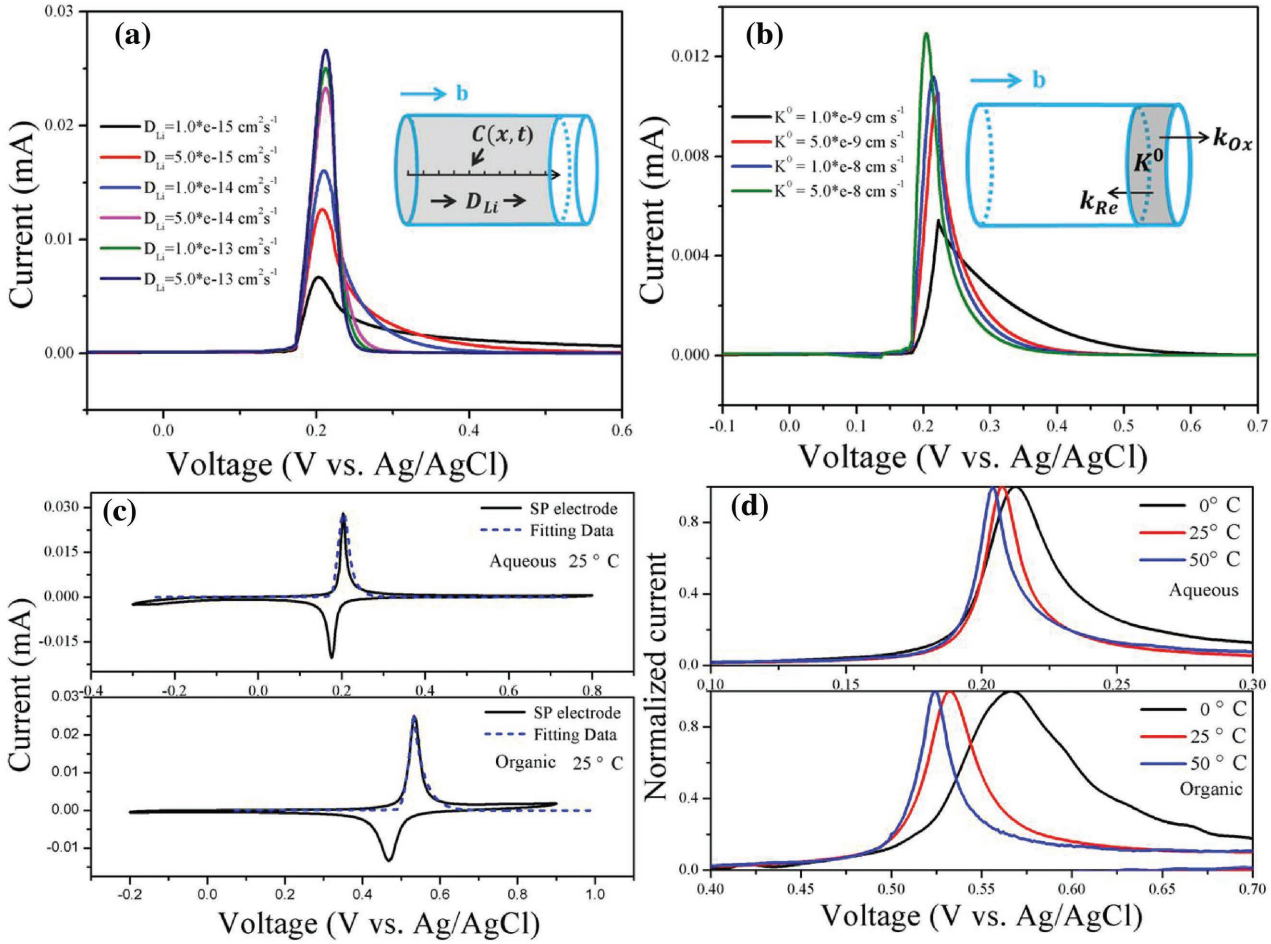

Figure 3. a) The variation tendency of CV curves with the increase of diffusion coefficient by SP-model. b) The variation tendency of CV curves with the increase of interfacial rate constant by SP-model. c) The CV curves of SP electrode and thick electrode in aqueous and organic electrolyte at 25 °C with the current density of 1 mV s^{-1}, the dotted lines are the simulation curves by the SP-model. d) The CV curves of SP electrode at different temperature in aqueous and organic electrolyte with the current density of 1 mV s^{-1}.

K^0. More importantly, through our SP-model (sphere model) (Figure S16, Supporting Information) by adjusting the related parameters, the simulated CV curves can be fitted perfectly well with the experimental cyclic voltammograms for the prepared $LiFePO_4$ SP electrode (Figure 3c) for the first time, and the obtained parameters were depicted in **Table 1**. (The exchange current density was expressed in Table S2, Supporting Information.) In order to verify our experimental method and SP model, we have done a compensatory experiment using CNT as the conductive network, the experiment data and final results are shown in Figure S17 and Table S3 of the Supporting Information, and the simulation results kept almost the same with those using carbon black as the conductive network. Moreover, we have also built a plate model. The lithium ion transport direction is b of $LiFePO_4$, and we calculated the length about the (010) face by Scherrer equation (27.3 nm). Combining with the above information, we took a simulation of the SP electrode under different temperature with different electrolytes (aqueous and organic). The simulation curves and data are shown in Figure S18 and Table S4 of the Supporting Information. The magnitude of diffusion coefficient and interfacial rate constant are also the same.

2.4. The Intrinsic Electrochemical Properties of Single $LiFePO_4$ Nanoparticles Derived from the Fitting Results of the SP Electrode Using the New SP Model

To further study temperature effects, we did the CV tests in different temperatures (0, 25, and 50 °C) at aqueous and organic electrolytes, respectively, to explore the electrochemical characteristics of $LiFePO_4$ (Figure 3d). In order to compare the change trend of CV curves in different temperature conveniently, we normalized it by dividing the maximum value of each CV data. It can be observed that the gradient of rising edge rises with the increasing temperature and the half-width becomes narrower, but there appears to be little difference in the trailing parts under different temperatures. In order to clarify this phenomenon, we measured electrochemical curves (Figures S19 and S20, Supporting Information) and did the electrochemical kinetics numerical simulations to fit the redox CV peaks obtained in different temperatures (Figures S21 and S22, Supporting Information). Table 1 shows the derived parameters. Note from Table 1 that when we increased diffusion coefficient to fit our CV data (more than 10^{-14} cm^2 s^{-1}), the simulation

Table 2. The signification and units of formula symbol.

Symbol	Signification	Units
i	Reaction current	A
E	Cathode potential	V
E^0	Standard potential	V
R	Universal gas constant	J mol^{-1} K^{-1}
T	Testing temperature	K
n	Quantity of exchange electron	
SOC	State of charge	
$C'(R_S, t)$	Vacancies concentration on surface of spherical particles	mol cm^{-3}
$C(R_S, t)$	Li-ions concentration on surface of spherical particles	mol cm^{-3}
K_{eq}	Equilibrium constant	
K_{Re}	Reduction reaction rate constant	cm s^{-1}
K_{Ox}	Oxidation reaction rate constant	cm s^{-1}
F	Faraday constant (96 487 C mol^{-1})	C mol^{-1}
A	Specific interfacial surface area	cm^2
K^0	Interfacial rate constant	cm s^{-1}
α	Symmetry factor	
D_{Li}	Li-ion diffusion coefficient	cm^2 s^{-1}

curves kept almost same (Figure 3a), which could be explained by the unconspicuous concentration polarization. Herein, we can propose that the diffusion coefficient of $LiFePO_4$ is higher than 10^{-14} cm^2 s^{-1}. In addition, the Li-ion diffusion coefficient of $LiFePO_4$ keeps almost the same both in aqueous and organic electrolyte in different temperatures. By contrast, the interfacial rate constant of $LiFePO_4$ shows large differences in aqueous and organic electrolyte. The interfacial rate constant of aqueous electrolyte is one order higher than that in organic electrolyte under the same temperature, and the interfacial rate constant of $LiFePO_4$ is small in low temperature, which agrees with the lower rate performance of $LiFePO_4$ at low temperature.[22] According to the simulation data (Table 1) and our previous work,[15] we deduce that the interfacial rate constant should be the rate-determining factor, which explains the excellent rate performance in aqueous electrolyte for $LiFePO_4$. We also fitted the discharge process (Figure S23, Supporting Information), the relevant coefficients are nearly the same as those in charge process (Table 1).

Through linear fitting the K^0 versus temperature, which would coincide the interface kinetic Arrhenius equation ($\ln K^0 = \ln A\text{-}E_a/RT$, K^0: interfacial rate constant; E_a: activation energy; A: pre-exponential factor; R: molar gas constant; T: thermodynamic temperature) (Figures S24 and S25, Supporting Information), we can get E_a and A both in charge and discharge processes. Interestingly, we found that the activation energies

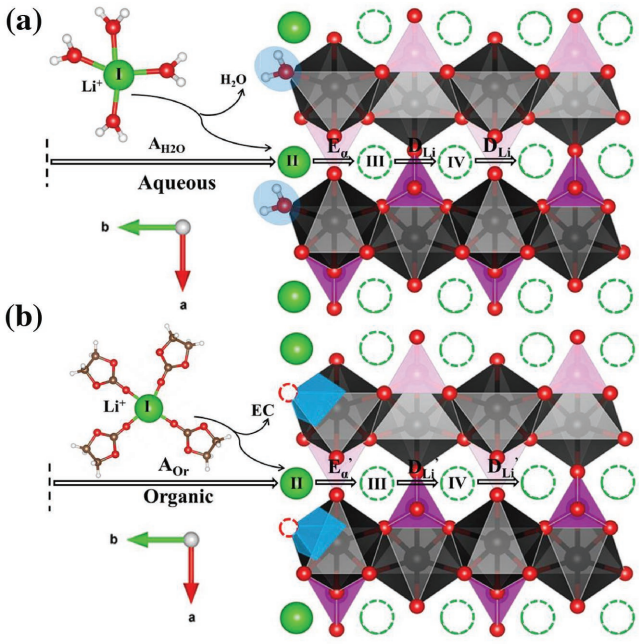

Figure 4. a,b) The interfacial reaction profiles for Li-ions transport across the $FePO_4$/water interface and $FePO_4$/EC interface in the discharge process.

in aqueous electrolyte are similar but a little higher than those in organic ($E\alpha(H_2O)$ = 38.66 ± 2 kJ mol^{-1}; $E\alpha'$ (organic) = 33.54 ± 2 kJ mol^{-1}, during charge process as shown in Figure S24, Supporting Information), so the almost one order larger interfacial rate constant in aqueous electrolyte can be attributed to the larger pre-exponential factor (A_{H2O} = 1.97*e^{-8}; A_{Or} = 2.96*e^{-9}). According to the Arrhenius equation, we can get E_a ($E\alpha$ = 39.74 ± 1 kJ mol^{-1}; $E\alpha'$ = 37.50 ± 1 kJ mol^{-1}) and A (A_{H2O} = 1.77*e^{-8}; A_{Or} = 2.95*e^{-9}) in the discharge process. To explain the above results, we depict the interfacial reaction and Li-ions diffusion profiles of $LiFePO_4$ in the charge and discharge process, as shown in Figure S26 of the Supporting Information and **Figure 4**, respectively. Taking the discharge process, for example, the interfacial reaction contains three steps: Li-ions jump from electrolyte to the surface of $LiFePO_4$ through a desolvation process, the attached surface Li-ions transport across the surface to the subsurface, and the Li-ions diffuse in the bulk $FePO_4$. The first step is mainly determined by the desolvation process, including the jumping path and the energy cost, which finally determines the pre-exponential factor A. The left two steps are mainly reflected by activation energy ($E\alpha$) and diffusion coefficient (D_{Li}), respectively. As the bulk $LiFePO_4$ is isolated from the electrolytes, the D_{Li} should be the same in both aqueous and organic electrolytes, as confirmed by the CV fitted data. According to our previous findings,[15] there is always a water molecule attached at the truncated corner of the surface FeO_6 octahedron in aqueous electrolytes (Figure 4a), thus leading to stronger binding of the surface Li. So the E_a of the surface Li-ions transport across the surface to the subsurface in aqueous electrolyte is a little higher than that in organic electrolyte, which explains that the larger value of E_a in aqueous electrolyte obtained from the CV fitting. By contrast,

the big difference for interfacial reaction of $LiFePO_4$ between aqueous and organic electrolytes comes from the desolvation process, as demonstrated by our previous calculations.[15] Each Li^+ in aqueous and organic electrolytes is always coordinated by four water and Ethylene Carbonate (EC) molecules in its primary solvation sheath, forming a complex cation $Li^+(H_2O)_4$ and $Li^+(EC)_4$, respectively. The $Li^+(H_2O)_4$ only needs to detach two water molecules to come to the $LiFePO_4$ surface due to the Janus solid–liquid interface, while the $Li^+(EC)_4$ needs to detach four EC molecules to come to the $LiFePO_4$ surface, thus leading to longer jumping path and costing more energy. This accounts for the much larger pre-exponential factor A in aqueous electrolyte compared with organic electrolyte.

3. Conclusion

We successfully prepared the SP electrode of $LiFePO_4$ nanocrystals and create new theoretical model for SP simulation to obtain the intrinsic electrochemical properties of $LiFePO_4$ nanocrystals. In order to make sure that our electrode can perform as a type of SP electrode, three important treatments are included as below: to take longer time for ultrasonic dispersing slurry to decrease agglomeration and minimize the interparticles interactions of active nanoparticles; to add optimized amount of conductive carbon or use CNT-networks to create electronic conductive networks to reduce the resistance for electrodes and to separate $LiFePO_4$ nanocrystal as single particle embedded in conductive carbon or CNT-networks; to form SP by making an ultrathin (only about 100–200 nm) electrode with a few layers of active nanoparticles ($LiFePO_4$) contacted with conductive carbon or CNT-network.

Because the traditional BV model failed to fit the ultrasharp CV peaks of the SP electrode due to $LiFePO_4$ feature with flat-voltage during the charge–discharge processes, we developed an improved SP-model to fit the experimental CV curves of SP $LiFePO_4$ perfectly. The novelty of the developed SP model is that the relationship between reaction rate and the voltage can be described precisely by learning the relationship from the real experimental potential-SOC curve of $LiFePO_4$ but not from the Nernst equation. Through fitting the sharp experimental CV peaks at different temperatures in different electrolytes, it is found that Li-ion diffusion coefficients of $LiFePO_4$ are nearly the same (higher than 10^{-14} cm^2 s^{-1}) in water and organic electrolytes, but the interfacial rate constant in aqueous electrolyte is much higher than organic electrolyte by one order and increases with the temperature. We propose for the first time that the insight of pre-exponential factor of interface kinetic Arrhenius equation is related to desolvation/solvation process. As a result, the higher interfacial rate constant in aqueous electrolyte is due to the much larger pre-exponential factor, because the desolvation process is much easier for Li-ions jumping from aqueous electrolyte to the surface of $LiFePO_4$. This work not only provides a new method to get the intrinsic electrochemical properties of $LiFePO_4$ particles and new SP-model to describe the electrochemical kinetics of SP electrode, but also gives a deep insight of the differences for the interfacial reactions in aqueous and organic electrolytes for $LiFePO_4$ nanocrystals.

4. Experimental Section

4.1. Preparation of $LiFePO_4$@C

$LiFePO_4$ nanocrystals were synthesized by reflux method. $FeSO_4{\cdot}7H_2O$ (AR, 99%), H_3PO_4 (AR, 85% solution), and $LiOH{\cdot}H_2O$ (AR, 95%) were dissolved in ethylene glycol (AR, 99%) as the original materials at room temperature, and the mole ratio of these substances was 1:1.275:2.7. First, the H_3PO_4 and LiOH solution were orderly added into the flask drop by drop with continuous stirring under nitrogen. Second, $FeSO_4$ solution dissolved with L-ascorbic acid (AR, 85%) was poured into the flask. After 30 min stirring, the mixed solution was heated to 180 °C and kept for 4 h. Third, the reflux products were washed by water and alcohol for three times and dried in vacuum at 70 °C for 3 h. Finally, the dried samples were ground with a certain amount of glucose (18.5 wt%) and V_c (1.5 wt%) and calcined at 650 °C for 6 h under Ar atmosphere, then we got $LiFePO_4$@C nanocrystals.

4.2. Characterization, SP Electrode Formation, and Electrochemical Measurements

The crystal structure of $LiFePO_4$@C samples was analyzed by X-ray diffraction using a Bruker D8-Advantage powder diffractometer (Cu-Kα radiation) from $2\theta = 0°$–$90°$ at 1s per step of 0.02°. The morphology of the samples was investigated by a SEM (ZEISS SURPA 55) operated at 5 kV. CV measurements were recorded by a CHI electrochemistry workstation (CHI604E series). The electrode materials distribution and height were detected by 3D confocal microscopy (vk-x200). The electrode materials were made up by mixing the $LiFePO_4$ nanocrystals (9 mg), carbon black or carbon nanotube (6 mg), and nafion (0.15 g) as binder into N-methyl-2-pyrrolidone (NMP) solution and ultrasound for different time (5, 25, 50, and 70 min), then dropped a very little amount of slurry on quartz monitor crystals (about 0.3 mg electrode materials on working electrode, when this amount of electrode materials were spread uniformly on the quartz monitor crystals, we could realize the 100 nm thickness of SP electrode). We took the three-electrode system to detect the electrochemical properties of a SP electrode of signal $LiFePO_4$ nanocrystals (Section S3 and Scheme S1, Supporting Information). The platinum electrode and Ag/AgCl were used as counter electrode and reference electrode, respectively. There are two kinds of electrolyte to detect the property of $LiFePO_4$ SP electrodes, aqueous solvent (0.5 M Li_2SO_4) and organic solvent (1 M $LiClO_4$ dissolved in Dimethyl Carbonate (DMC)/EC with volume ratio of 1:1), respectively. Tests were conducted in the potential range of −0.3 to 0.8 V in aqueous electrolyte and −0.2 to 0.9 V in organic electrolyte (vs Ag/AgCl).

4.3. Butler–Volmer Model, Marcus–Hush–Chidsey Theory Model, and Single-Particle Model

In order to inquiry the intrinsic properties of $LiFePO_4$ by eliminating the internal interference such as concentration, polarization, ohmic polarization,[18] interparticle charging and discharging[23] as far as possible, we directly focus on each $LiFePO_4$ particle and utilize the single-particle model. We take the $LiFePO_4$ active material as a separate nanosized sphere in which the Li-ions diffuse along b-axis,[21,24] which are evenly coated on the electrode to form an ultrathin SP electrode. The solid phase is assumed to comprise of identical spherical particles of a predetermined size, and diffusion in the *b*-axis direction is assumed to be the predominant mode of transport. The diffusion process satisfies the Fick's law and the related boundary conditions, and the interface charge transfer process are described by the standard Butler–Volmer equation, Marcus–Hush–Chidsey theory, and our novel SP-model for thick and SP-electrodes, respectively.

4.3.1. BV Model

As for the process of discharge at the cathode, $LiFePO_4 \rightarrow FePO_4^- + Li^+$, almost all the previous literatures use the porous-electrode cell model that accord with the BV equation to describe it. In order to simplify the model we assumed that the reaction just takes place at the solid and liquid phase process and does not generate gas. The active materials in the positive electrode can be modeled as spheres of radius R_s which is kept constant in the whole process. Besides, the heat coupled with the reaction can be ignored and Li-ion diffusion coefficient has no relation with the SOC. The formula symbol appeared in the BV model and the MHC theory model was depicted in Table S1 of the Supporting Information.

So Li-ion in the solid phase is assumed to move via the Fick's diffusion law, as it is shown in Equation (7)

$$\frac{\partial C(x,t)}{\partial t} = \frac{D_{Li}}{x^2}\frac{\partial}{\partial x}\left(x^2\frac{\partial C(x,t)}{\partial x}\right) \tag{7}$$

And the boundary condition at the $x = R_s$ can be expressed as

$$\frac{i}{FA} = D_{Li}\left[\frac{\partial C(x,t)}{\partial x}\right]_{x=R_s} = k_f(t)C(R_s,t) - k_b(t)C'(R_s,t)^{\alpha}C^{s(1-\alpha)} \tag{8}$$

$$k_b(t) = k^0\exp\left\{-\alpha\frac{F}{RT}\left[E(t)-E^0\right]\right\} \tag{9}$$

$$k_f(t) = k^0\exp\left\{(1-\alpha)\frac{F}{RT}\left[E(t)-E^0\right]\right\} \tag{10}$$

Since the flux in the center of particle equals to zero, the other boundary condition is

$$D_{Li}\left[\frac{\partial C(x,t)}{\partial x}\right]_{x=0} = 0 \tag{11}$$

With different electrochemical parameters such as k^0, α, D_{Li}, and the boundary conditions we can use mathematical methods to solve the partial differential equation and to recreate a CV curve.

Rigorously, the measured current in the CV test is associated with four parts: Li-ions diffusion in the $LiFePO_4$ cathode, Li-ions transport across the cathode/electrolyte interface, Li-ions diffusion in the bulk electrolyte, and the IR drop. In our experiments, the last two factors are not the rate-limiting step. At the same time, the Li-ions diffusions inside or outside the $LiFePO_4$ nanoparticle should be independent from the electrolytes used, either aqueous or nonaqueous.

4.3.2. MHC Theory Model

Compared with traditional BV model, the biggest advantage of MHC theory model is that it can characterize the whole electrochemical kinetics process in the angle of microscopic. The physical mass transfer process and the boundary condition of the MHC model were identical with the BV model. We would not elaborate further here. As well as for the process of discharge at the $LiFePO_4$ similar single particle thin film electrode $LiFePO_4 \rightarrow FePO_4^- + Li^+$ the current of the reaction can be depicted by the equation (Equation (12))

$$i = FA\left[-K_{red}^{MHC}\tau_{red} + K_{ox}^{MHC}\tau_{ox}\right] \tag{12}$$

According to Marcus–Hush charge transfer equation, the reduction rate constant and the oxidation rate constant are

$$K_{red}^{MHC} = K_0^{MHC}\exp\left(-\frac{\theta}{2}\right)\frac{I(\delta,\theta)}{I(\delta,0)} \tag{13}$$

$$K_{ox}^{MHC} = K_0\exp\left(+\frac{\theta}{2}\right)\frac{I(\delta,\theta)}{I(\delta,0)} \tag{14}$$

The meaning of θ, δ, and $I(\delta, \theta)$ is

$$\theta = \frac{F}{RT}\left(E(t)-E_f^0\right) \tag{15}$$

$$\delta = \frac{F}{RT}\lambda \tag{16}$$

$$I(\delta,\theta) = \int_{-\infty}^{\infty}\frac{\exp\left(\frac{-(\epsilon-\theta)^2}{4\delta}\right)}{2\cosh\left(\frac{\epsilon}{2}\right)}d\epsilon \tag{17}$$

With different electrochemical parameters and the boundary conditions we can use mathematical methods to solve the partial differential equation and to recreate a CV curve. We explore the effects of all parameters on the shape of the fitted curve and found that only $K^{MHC}{}_0$ can change the slope of the rising edge of the CV curves.

4.3.3. SP-Model

The physical mass transfer process and the boundary condition of SP-model were identical with the BV model. We would not elaborate further here. Careful analysis the curve drawn by the Nernst equation and discharge curve of $LiFePO_4$ diagram, such as in Figure S15a of the Supporting Information, we can find that the two were not consistent. Due to the kind of single particle experiment under the condition of Li-ions diffusion in the solution very fast, we temporarily do not consider Li-ions concentration in solution phase and just consider the Li-ions concentration in solid phase. For most materials such as $LiCoO_2$ or ternary materials, the shape of potential versus SOC is like the red line in Figure S15a of the Supporting Information. The line can be calculated from Nernst equation, i.e.,

$$E = E^0 + \frac{RT}{nF}\ln\frac{(1-SOC)}{SOC} = E^0 + \frac{RT}{nF}\ln\frac{C(R_s,t)}{C'(R_s,t)} \tag{18}$$

The formula symbol appeared in the SP-model and its signification and units will be depicted in **Table 2**.

The equilibrium constant, i.e., ration of concentration of Li-ions and hole at any given potential E can be calculated from Equation (19). The equilibrium constant can also be represented by the ratio of oxidation and reduction reaction rate constant

$$K_{eq} = \frac{C(R_s,t)}{C'(R_s,t)} = \frac{K_{Ox}}{K_{Re}} = e^{\frac{nF}{RT}(E-E^0)} \tag{19}$$

We cannot obtain the individual oxidation and reduction rate constant from this equation. We need another hypothesis that is the relationship between active energy and over potential. We got next equation

$$\frac{K_{Ox}}{K_{Re}} = \frac{K^0 e^{\frac{(1-\alpha)nF}{RT}(E-E^0)}}{K^0 e^{-\frac{\alpha nF}{RT}(E-E^0)}} \tag{20}$$

$$K_{Ox} = K^0 e^{\frac{(1-\alpha)nF}{RT}(E-E^0)} \quad (21)$$

$$K_{Re} = K^0 e^{-\frac{\alpha nF}{RT}(E-E^0)} \quad (22)$$

For $LiFePO_4$ Equations (21) and (22) of oxidation and reduction reaction rate constant are not available. However, the next expression is still true

$$K_{eq} = \frac{K_{Ox}}{K_{Re}} = \frac{C(R_s,t)}{C'(R_s,t)} = \frac{(1-SOC)}{SOC} \quad (23)$$

For the sake of calculating more conveniently, based on the discharge curve tested in different electrolyte at different temperature (the discharge curve tested at 0, 25, 50 °C in both aqueous and nonaqueous were shown in Figure 2c and Figures S19 and S20, Supporting Information), though a simple conversion we can get the relationship between K_{eq} and the potential in different electrolyte at different conditions (the discharge curve tested at 25 °C in both aqueous and nonaqueous after conversion were shown in Figure S16, Supporting Information). Finally, we submit the obtained relationship $K_{eq} = f(E)$ into Formula (24) and can get the reaction current as

$$i = FAK^0\left[C(R_s,t)10^{(1-\alpha)\log_{10} f(E)} - C'(R_s,t)10^{-\alpha\log_{10} f(E)}\right] \quad (24)$$

Use these relationships and formulas we can simulate the CV curves tested in different condition.

Supporting Information

Supporting Information is available from the Wiley Online Library or from the author.

Acknowledgements

J.H. and W.L. contributed equally to this work. The research was financially supported by Guangdong Innovation Team Project (No. 2013N080), Shenzhen Science and Technology Research Grant (peacock plan KYPT20141016105435850, No. JCYJ20140903101617271) and National Materials Genome Project (2016YFB0700600).

Received: August 27, 2016
Revised: September 23, 2016
Published online: November 17, 2016

[1] a) F. Zhou, K. Kang, T. Maxisch, G. Ceder, D. Morgan, *Solid State Commun.* **2004**, *132*, 181; b) S. Y. Chung, J. T. Bloking, Y. M. Chiang, *Nat. Mater.* **2002**, *1*, 123; c) L. Wang, X. He, W. Sun, J. Wang, Y. Li, S. Fan, *Nano Lett.* **2012**, *12*, 5632; d) K. Zaghib, A. Guerfi, P. Hovington, A. Vijh, M. Trudeau, A. Mauger, J. B. Goodenough, C. M. Julien, *J. Power Sources* **2013**, *232*, 357.
[2] L. Kyu Tae, H. Wang, Kan, L. F. Nazar, *J. Am. Chem. Soc* **2009**, *131*, 6044.
[3] J. Maier, *Nat. Mater.* **2005**, *4*, 805.
[4] a) D. A. Cogswell, M. Z. Bazant, *ACS Nano* **2012**, *6*, 2215; b) D. A. Cogswell, M. Z. Bazant, *Nano Lett.* **2013**, *13*, 3036.
[5] J. Hu, Y. Jiang, S. Cui, Y. Duan, T. Liu, H. Guo, L. Lin, Y. Lin, J. Zheng, K. Amine, F. Pan, *Adv. Energy Mater.* **2016**, *6*, 1600856.
[6] W. C. Chueh, F. El Gabaly, J. D. Sugar, N. C. Bartelt, A. H. McDaniel, K. R. Fenton, K. R. Zavadil, T. Tyliszczak, W. Lai, K. F. McCarty, *Nano Lett.* **2013**, *13*, 866.
[7] G. Brunetti, D. Robert, P. Bayle-Guillemaud, J. L. Rouvière, E. F. Rauch, J. F. Martin, J. F. Colin, F. Bertin, C. Cayron, *Chem. Mater.* **2011**, *23*, 4515.
[8] Y. Li, J. N. Weker, W. E. Gent, D. N. Mueller, J. Lim, D. A. Cogswell, T. Tyliszczak, W. C. Chueh, *Adv. Funct. Mater.* **2015**, *25*, 3677.
[9] D. Robert, T. Douillard, A. Boulineau, G. Brunetti, P. Nowakowski, D. Venet, P. Bayle-Guillemaud, C. Cayron, *ACS Nano* **2013**, *7*, 10887.
[10] J. Lim, Y. Li, D. H. Alsem, H. So, S. C. Lee, P. Bai, D. A. Cogswell, X. Liu, N. Jin, Y.-S. Yu, N. J. Salmon, D. A. Shapiro, M. Z. Bazant, T. Tyliszczak, W. C. Chueh, *Science* **2016**, *353*, 566.
[11] S. Ling, J. Wu, S. Zhang, J. Gao, S. Wang, H. Li, *Energy Storage Sci. Technol.* **2015**, *4*, 83.
[12] S. R. Das, S. B. Majumder, R. S. Katiyar, *J. Power Sources* **2005**, *139*, 261.
[13] S. Liumin, B. Oleg, G. Tao, O. Marco, H. Janet, F. Xiulin, L. Chao, W. Chunsheng, X. Kang, *Science* **2015**, *350*, 938.
[14] a) T. Liu, Y. Feng, Y. Duan, S. Cui, L. Lin, J. Hu, H. Guo, Z. Zhuo, J. Zheng, Y. Lin, W. Yang, K. Amine, F. Pan, *Nano Energy* **2015**, *18*, 187; b) T. Liu, Y. Duan, G. Zhang, M. Li, Y. Feng, J. Hu, J. Zheng, J. Chen, F. Pan, *J. Mater. Chem. A* **2016**, *4*, 4479.
[15] J. Zheng, Y. Hou, Y. Duan, X. Song, Y. Wei, T. Liu, J. Hu, H. Guo, Z. Zhuo, L. Liu, Z. Chang, X. Wang, D. Zherebetskyy, Y. Fang, Y. Lin, K. Xu, L. W. Wang, Y. Wu, F. Pan, *Nano Lett.* **2015**, *15*, 6102.
[16] a) M. C. Henstridge, C. Batchelor-McAuley, R. Gusmão, R. G. Compton, *Chem. Phys. Lett.* **2011**, *517*, 108; b) M. C. Henstridge, E. Laborda, R. G. Compton, *J. Electroanal. Chem.* **2012**, *674*, 90; c) M. C. Henstridge, E. Laborda, N. V. Rees, R. G. Compton, *Electrochim. Acta* **2012**, *84*, 12.
[17] H. Fei, Z. Peng, Y. Yang, L. Li, A. R. Raji, E. L. Samuel, J. M. Tour, *Chem. Commun.* **2014**, *50*, 7117.
[18] A. J. Bard, L. R. Faulkner, *Electrochemical Methods: Fundamentals and Applications*, John Wiley & Sons, Inc., New York **2000**.
[19] C. G. Zoski, *Handbook of Electrochemistry*, Elsevier, **2007**.
[20] Y. Wei, J. Zheng, S. Cui, X. Song, Y. Su, K. Amine, F. Pan, *J. Am. Chem. Soc*, **2015**, *137*, 8364.
[21] R. Malik, A. Abdellahi, G. Ceder, *J. Electrochem. Soc.* **2013**, *160*, A3179.
[22] G. Cai, R. Guo, L. Liu, Y. Yang, C. Zhang, C. Wu, W. Guo, H. Jiang, *J. Power Sources* **2015**, *288*, 136.
[23] Y. Li, S. Meyer, J. Lim, S. C. Lee, W. E. Gent, S. Marchesini, H. Krishnan, T. Tyliszczak, D. Shapiro, A. L. D. Kilcoyne, W. C. Chueh, *Adv. Mater.* **2015**, *27*, 6590.
[24] J. Wang, X. Sun, *Energy Environ. Sci.* **2012**, *5*, 5163.